Mon. Not. R. Astron. Soc. **399,** 1482–1494 (2009) doi:10.1111/j.1365-2966.2009.15363.x

The initial shear field in models with primordial local non-Gaussianity and implications for halo and void abundances

Tsz Yan Lam,[1,2⋆] Ravi K. Sheth[1⋆] and Vincent Desjacques[3⋆]

[1] *Center for Particle Cosmology, University of Pennsylvania, 209 S. 33rd Street, Philadelphia, PA 19104, USA*
[2] *Institute for the Physics and Mathematics of the Universe, University of Tokyo, Chiba 277-8582, Japan*
[3] *Institute for Theoretical Physics, University of Zürich, Winterthurerstrasse 190, CH-8057 Zürich, Switzerland*

Accepted 2009 July 7. Received 2009 July 7; in original form 2009 May 11

ABSTRACT

We generalize the Doroshkevich's celebrated formulae for the eigenvalues of the initial shear field associated with Gaussian statistics to the local non-Gaussian f_{nl} model. This is possible because, to at least second order in f_{nl}, distributions at fixed overdensity are unchanged from the case $f_{nl} = 0$. We use this generalization to estimate the effect of $f_{nl} \neq 0$ on the abundance of virialized haloes. Halo abundances are expected to be related to the probability that a certain quantity in the initial fluctuation field exceeds a threshold value, and we study two choices for this variable: it can either be the sum of the eigenvalues of the initial deformation tensor (the initial overdensity) or its smallest eigenvalue. The approach based on a critical overdensity yields results which are in excellent agreement with numerical measurements. We then use these same methods to develop approximations describing the sensitivity of void abundances on f_{nl}. While a positive f_{nl} produces more extremely massive haloes, it makes fewer extremely large voids. Its effect thus is qualitatively different from a simple rescaling of the normalization of the density fluctuation field σ_8. Therefore, void abundances furnish complementary information to cluster abundances, and a joint comparison of both might provide interesting constraints on primordial non-Gaussianity.

Key words: methods: analytical – large-scale structure of Universe.

1 INTRODUCTION

Detections of non-Gaussianity can discriminate between different inflation models (e.g. Maldacena 2003). The local f_{nl} model, where the primordial perturbation potential is

$$\Phi = \phi + f_{nl}(\phi^2 - \langle\phi^2\rangle), \tag{1}$$

where ϕ is a Gaussian potential field and f_{nl} is a scalar, this has been the subject of much recent study (e.g. Buchbinder, Khoury & Ovrut 2008; Khoury & Piazza 2009; Silvestri & Trodden 2008, and references therein). Constraints on this model tend to be of two types – from the CMB (Hikage et al. 2008; McEwen et al. 2008; Yadav & Wandelt 2008; Komatsu et al. 2009; Rossi et al. 2009) and from large-scale structures in the Universe (Koyama, Soda & Taruya 1999; Matarrese, Verde & Jimenez 2000; Scoccimarro, Sefusatti & Zaldarriaga 2004; Izumi & Soda 2007; Sefusatti & Komatsu 2007; Afshordi & Tolley 2008; Carbone, Verde & Matarrese 2008; Dalal et al. 2008; Desjacques, Seljak & Iliev 2009; Grossi et al. 2008; Lo Verde et al. 2008; Matarrese & Verde 2008; McDonald 2008; Pillepich, Porciani & Hahn 2008; Slosar et al. 2008; Taruya, Koyama & Matsubara 2008; Grossi et al. 2009; Kamionkowski, Verde & Jimenez 2009; Lam & Sheth 2009b; Slosar 2009).

The initial shear field is expected to play an important role in the formation of large-scale structures (Zel'Dovich 1970; Bond & Myers 1996; Lee & Shandarin 1998, hereafter LS; Sheth, Mo & Tormen 2001; Bernardeau et al. 2002; Desjacques 2008). The main goal of the present work is to show that much of the machinery developed for the study of structure formation from Gaussian initial conditions can be carried over, with minor modifications, to the study of f_{nl} models. We do so by showing how to generalize the Doroshkevich's celebrated formulae for the eigenvalues of the initial shear field associated with Gaussian statistics (Doroshkevich 1970) to the local non-Gaussian f_{nl} model.

⋆E-mail: tylam@sas.upenn.edu (TYL); shethrk@physics.upenn.edu (RKS); dvince@physik.uzh.ch (VD)

We then study how the abundance of virialized dark matter haloes depend on f_{nl}. This study focuses on two problems: one is the physical model for halo formation, and the other is the statistical problem of how this collapse model is used to estimate the abundance of such collapsed objects. We use the approach pioneered by Press & Schechter (1974) (hereafter PS) and refined by Bond et al. (1991) to address the statistical problem (see Maggiore & Riotto 2009a; Lam & Sheth 2009a, for recent extensions which treat the $f_{nl} \neq 0$ case). We study two different models for the physics of halo formation: one in which haloes form from sufficiently overdense regions in the initial fluctuation field (PS; Sheth et al. 2001), and another in which the criterion for halo formation is that all three eigenvalues of the initial deformation tensor exceed a certain value (e.g. LS). In the former, we use the triaxial collapse model of Bond & Myers (1996) to estimate this critical overdensity (following Sheth et al. 2001). If our way of estimating halo abundances are reliable, then comparison with simulations run for a range of f_{nl} values provides a novel way to study the physics of gravitational clustering.

Section 2 provides explicit expressions for the initial eigenvalue distribution, and for the initial distribution of the variables which arise naturally in the context of triaxial collapse models. These are used, in Section 3, to estimate how the mass function of virialized objects is modified when $f_{nl} \neq 0$. This section also shows the result of comparing these estimates with measurements in simulations. With some care (e.g. Sheth & van de Weygaert 2004), much of the analysis can be carried over straightforwardly to study void abundances; this is the subject of Section 4. A final section summarizes our results. An Appendix describes an alternative estimate of halo abundances which is logically consistent with previous work, but which does not reproduce the f_{nl} dependence seen in simulations.

2 THE LOCAL NON-GAUSSIAN MODEL

We are interested in models where the primordial perturbation potential is given by equation (1). We will use $P_\phi(k)$ to represent the power spectrum of ϕ; in what follows, we will set $P_\phi(k) = Ak^{n_s-4}$, where $n_s \approx 1$, and A is a normalization constant that is fixed by requiring that the rms fluctuation in the associated non-Gaussian initial density field (which we will define shortly) has value σ_8. The power spectrum and bispectrum of the Φ field are

$$P_\Phi(k) = P_\phi(k) + \frac{2f_{nl}^2}{(2\pi)^3}\int \mathrm{d}\boldsymbol{q}\,\left[P_\phi(q)P_\phi(|\boldsymbol{k}-\boldsymbol{q}|) - P_\phi(k)P_\phi(q) - P_\phi(k)P_\phi(|\boldsymbol{k}-\boldsymbol{q}|)\right], \tag{2}$$

$$B_\Phi(k_1,k_2,k_{12}) \equiv 2f_{nl}\,\left[P_\phi(k_1)P_\phi(k_2) + \mathrm{cyclic}\right] + \mathcal{O}\left(f_{nl}^3\right) \tag{3}$$

(Scoccimarro et al. 2004).

2.1 The shear or deformation tensor

Define $\boldsymbol{D}$ as the real, symmetric 3×3 tensor whose components are proportional to the second order derivatives of the potential Φ:

$$\Phi_{ij} \equiv \phi_{ij} + 2f_{nl}(\phi_i\phi_j + \phi\phi_{ij}), \tag{4}$$

where $\phi_i = \partial_i\,\phi$ and $\phi_{ij} = \partial_i\partial_j\phi$. We will sometimes refer to $\boldsymbol{D}$ as the shear field associated with the potential Φ. Correlations between the Φ_{ij} will be very useful in what follows. These depend on the correlations between ϕ and its derivatives but, because ϕ is Gaussian, they can be computed easily. Doing so shows that the six components of $\boldsymbol{D}$ are not independent: although the three off-diagonal terms are not correlated with the others, the three diagonal terms are. However, if we set

$$x = \sum_i \Phi_{ii}, \qquad y = \frac{1}{2}(\Phi_{11}-\Phi_{22}), \qquad z = \frac{1}{2}(\Phi_{11}+\Phi_{22}-2\Phi_{33}), \tag{5}$$

then these three parameters, combined with (Φ_{12}, Φ_{23}, Φ_{31}), form a new set of six independent components (Bardeen et al. 1986). When $f_{nl} = 0$, then each of these is an independent Gaussian random field.

Most of the complication in f_{nl} models arises from the fact that we are almost always interested in spatially smoothed quantities. Fortunately, smoothing is a linear operation, and the new variables x, y, z are just linear combinations of the elements of $\boldsymbol{D}$. Hence, if $W(kR)$ denotes the Fourier transform of the smoothing window of scale R, to second order in f_{nl},

$$\langle x^2\rangle = \sigma^2, \qquad \langle y^2\rangle = \frac{\sigma^2}{15}, \qquad \langle z^2\rangle = \frac{\sigma^2}{5}, \qquad \left\langle \Phi_{ij}^2\right\rangle_{i\neq j} = \frac{\sigma^2}{15}, \tag{6}$$

$$\langle x^3\rangle = 2f_{nl}\gamma^3 \qquad \langle y^3\rangle = 0 \qquad \langle z^3\rangle = 0 \qquad \left\langle \Phi_{ij}^3\right\rangle_{i\neq j} = 0, \tag{7}$$

where

$$\sigma^2 = \frac{1}{(2\pi)^3}\int \frac{\mathrm{d}k}{k} 4\pi\, k^7 M^2(k)\, P_\Phi(k)\, W^2(kR), \tag{8}$$

$$\gamma^3 = \frac{2}{(2\pi)^4}\int \frac{\mathrm{d}k_1}{k_1} k_1^5 M(k_1)W(k_1R)\int \frac{\mathrm{d}k_2}{k_2} k_2^5 M(k_2)W(k_2R)\int \mathrm{d}\mu_{12}\, k_{12}^2\, M(k_{12})W(k_{12}R)\frac{B_\Phi(k_1,k_2,k_{12})}{2f_{nl}} \tag{9}$$

and $M(k) \equiv (3D(z)c^2)/(5\Omega_m\, H_0^2)\,T(k)$, where $T(k)$ is the cold dark matter transfer function and $D(z)$ is the linear growth function. In what follows, the quantity $\sigma S_3 \equiv \sigma\,\langle x^3\rangle/\langle x^2\rangle^2$ will play an important role, because it represents the leading order contribution to the non-Gaussianity (note that it is proportional to f_{nl}). Appendix A in Lam & Sheth (2009a) provides a useful fitting formula for this quantity.

2.2 Joint distribution of eigenvalues

Equation (7) shows that, to first order in f_{nl}, five of the six parameters have zero skewness, so, to first order in f_{nl}, all but x are drawn from Gaussian distributions. However, x is the trace of $\boldsymbol{D}$, so it is the linear theory overdensity δ. If $p(\delta|R)$ denotes the distribution of δ when smoothed on scale R, then the fact that the other variables have the same distribution as in the case $f_{nl} = 0$ allows one to provide an excellent analytic approximation to the joint distribution of the eigenvalues. Namely,

$$p(\boldsymbol{\lambda}|R) = p(\delta|R)\,\frac{3^4/4}{\Gamma(5/2)}\left(\frac{5}{2\sigma^2}\right)^{5/2}\exp\left(-\frac{5\delta^2}{2\sigma^2}+\frac{15I}{2\sigma^2}\right)(\lambda_1-\lambda_2)(\lambda_2-\lambda_3)(\lambda_1-\lambda_3), \tag{10}$$

where $\delta \equiv \lambda_1+\lambda_2+\lambda_3$, $I \equiv \lambda_1\lambda_2+\lambda_1\lambda_3+\lambda_2\lambda_3$, and recall that σ is a function of R. Our convention is $\lambda_1 \geq \lambda_2 \geq \lambda_3$. This has the same form as the Doroshkevich's (1970) formula for Gaussian fields; the only difference is that here $p(\delta|R)$ is not Gaussian (we provide an expression for it in equation 13 below).

The fundamental reason why this works is that the Doroshkevich's formula is actually the product of two independent distributions, one of δ and the other of a quantity which is a combination of the five other independent elements of the deformation tensor (e.g. Sheth & Tormen 2002). Since the distribution of each of these other elements is unchanged from the Gaussian case (we just showed that they all have zero skewness), this second distribution is unchanged from that of the Gaussian case – the only change is the distribution of δ. In fact, this holds for any local mapping $\Phi = f(\phi)$ (and is also true for the alignment of the principal axes, see Desjacques & Smith 2008).

2.3 Distributions at fixed δ

One consequence of this is that distributions at fixed δ are the same as in the Gaussian case. For example,

$$p(\lambda_i,\lambda_j|\delta) = \frac{3^4/4}{\Gamma(5/2)}\left(\frac{5}{2\sigma^2}\right)^{5/2}\exp\left(-\frac{5\delta^2}{2\sigma^2}+\frac{15I_{ij}}{2\sigma^2}\right)(\lambda_i-\lambda_j)(\lambda_i+2\lambda_j-\delta)(2\lambda_i+\lambda_j-\delta) = p_0(\lambda_i,\lambda_j|\delta), \tag{11}$$

where $i \neq j$ can take values from 1 to 3, $I_{ij} = \lambda_i\lambda_j+(\lambda_i+\lambda_j)(\delta-\lambda_i-\lambda_j) = \delta(\lambda_i+\lambda_j)-(\lambda_i^2+\lambda_i\lambda_j+\lambda_j^2)$, and the subscript 0 indicates the distribution associated with Gaussian initial conditions, for which $f_{nl} = 0$. Integrating over one of the eigenvalues in the expression above, e.g. λ_i, yields an expression for the distribution of the other at fixed δ. Clearly, such expressions will also be the same as in the Gaussian case. Hence,

$$p(\lambda_j|\delta) = p_0(\lambda_j|\delta) \tag{12}$$

for $j = 1, 2, 3$.

2.4 Edgeworth approximation for $p(\delta|R)$

Because we are interested in small departures from Gaussianity, the Edgeworth expansion provides a convenient form for the distribution of δ:

$$p(\delta|R)\,\mathrm{d}\delta \approx \left[1+\frac{\sigma(R)S_3(R)}{6}H_3\left(\frac{\delta}{\sigma(R)}\right)\right]\frac{\mathrm{e}^{-\delta^2/2\sigma^2(R)}}{\sqrt{2\pi}\sigma(R)}\,\mathrm{d}\delta = \left[1+\frac{\sigma S_3}{6}H_3(\nu)\right]p_0(\delta|R)\,\mathrm{d}\delta, \tag{13}$$

where $\sigma(R)$ is given by equation (8), $\sigma S_3 \equiv \langle x^3\rangle/\langle x^2\rangle^{3/2} = 2f_{nl}\,\gamma^3/\sigma^3$, and $H_3(\nu) \equiv \nu(\nu^2-3)$ with $\nu \equiv \delta/\sigma(R)$ (see Lo Verde et al. 2008 and Lam & Sheth 2009b for previous work with the Edgeworth expansion in the context of f_{nl} models.) The final equality writes p as a correction factor times the Gaussian distribution p_0 to highlight the fact that

$$p(\boldsymbol{\lambda}|R) = \left[1+\frac{\sigma S_3}{6}H_3\left(\delta/\sigma\right)\right]p_0(\boldsymbol{\lambda}|R)\,, \tag{14}$$

where $p_0(\boldsymbol{\lambda}|R)$ is the Doroshkevich's formula.

2.5 Distribution of eigenvalues

Replacing $p(\delta|R)$ in equation (10) by its Edgeworth expansion and integrating over two of the three eigenvalues, we can write

$$p(\lambda_i) = p_0(\lambda_i)+\frac{\sigma S_3}{6}\,\Delta p(\lambda_i), \tag{15}$$

where

$$\begin{aligned} p_0(\lambda_1) = \frac{\sqrt{5}}{12\pi\sigma}\Bigg\{&20\frac{\lambda_1}{\sigma}\exp\left(-\frac{9\lambda_1^2}{2\sigma^2}\right)-\sqrt{2\pi}\exp\left(-\frac{5\lambda_1^2}{2\sigma^2}\right)\left(1-20\frac{\lambda_1^2}{\sigma^2}\right)\left[1+\mathrm{erf}\left(\sqrt{2}\frac{\lambda_1}{\sigma}\right)\right]\\ &+3\sqrt{3\pi}\exp\left(-\frac{15\lambda_1^2}{4\sigma^2}\right)\left[1+\mathrm{erf}\left(\frac{\sqrt{3}\lambda_1}{2\sigma}\right)\right]\Bigg\},\\ p_0(\lambda_2) = \frac{\sqrt{15}}{2\sqrt{\pi}\sigma}\exp\left(-\frac{15\lambda_2^2}{4\sigma^2}\right),& \end{aligned} \tag{16}$$

$$p_0(\lambda_3) = -\frac{\sqrt{5}}{12\pi\sigma}\left[20\frac{\lambda_3}{\sigma}\exp\left(-\frac{9\lambda_3^2}{2\sigma^2}\right)+\sqrt{2\pi}\exp\left(-\frac{5\lambda_3^2}{2\sigma^2}\right)\mathrm{erfc}\left(\sqrt{2}\frac{\lambda_3}{\sigma}\right)\left(1-20\frac{\lambda_3^2}{\sigma^2}\right)\right.$$
$$\left.-3\sqrt{3\pi}\exp\left(-\frac{15\lambda_3^2}{4\sigma^2}\right)\mathrm{erfc}\left(\frac{\sqrt{3}\lambda_3}{2\sigma}\right)\right] \quad (17)$$

and

$$\Delta p(\lambda_1) = \frac{\sqrt{5}}{12\pi\sigma}\left\{\frac{25}{27}\left(8-\frac{435\lambda_1^2}{4\sigma^2}+100\frac{\lambda_1^4}{\sigma^4}\right)\exp\left(-\frac{9\lambda_1^2}{2\sigma^2}\right)+\sqrt{2\pi}\frac{25\lambda_1}{27\sigma}\left(51-185\frac{\lambda_1^2}{\sigma^2}+100\frac{\lambda_1^4}{\sigma^4}\right)\exp\left(-\frac{5\lambda_1^2}{2\sigma^2}\right)\left(1+\mathrm{erf}\left(\sqrt{2}\frac{\lambda_1}{\sigma}\right)\right)\right.$$
$$\left.+3\sqrt{3\pi}\frac{25\lambda_1}{4\sigma}\left(\frac{5\lambda_1^2}{2\sigma^2}-1\right)\exp\left(-\frac{15\lambda_1^2}{4\sigma^2}\right)\left[1+\mathrm{erf}\left(\frac{\sqrt{3}\lambda_1}{2\sigma}\right)\right]\right\}, \quad (18)$$

$$\Delta p(\lambda_2) = \left(\frac{5}{6}\right)^{3/2}\frac{\sqrt{15}\lambda_2}{\sqrt{2}\sigma}\left(\frac{15\lambda_2^2}{2\sigma^2}-3\right)\,p_0(\lambda_2) = \left(\frac{5}{6}\right)^{3/2}H_3\left(\frac{\sqrt{15}\lambda_2}{\sqrt{2}\sigma}\right)\,p_0(\lambda_2), \quad (19)$$

$$\Delta p(\lambda_3) = \frac{\sqrt{5}}{12\pi\sigma}\left[-\frac{25}{27}\left(8-\frac{435}{4}\frac{\lambda_3^2}{\sigma^2}+100\frac{\lambda_3^4}{\sigma^4}\right)\exp\left(-\frac{9\lambda_3^2}{2\sigma^2}\right)+\sqrt{2\pi}\frac{25\lambda_3}{27\sigma}\left(51-185\frac{\lambda_3^2}{\sigma^2}+100\frac{\lambda_3^4}{\sigma^4}\right)\exp\left(-\frac{5\lambda_3^2}{2\sigma^2}\right)\mathrm{erfc}\left(\sqrt{2}\frac{\lambda_3}{\sigma}\right)\right.$$
$$\left.+3\sqrt{3\pi}\frac{25\lambda_3}{4\sigma}\left(\frac{5\lambda_3^2}{2\sigma^2}-1\right)\exp\left(-\frac{15\lambda_3^2}{4\sigma^2}\right)\mathrm{erfc}\left(\frac{\sqrt{3}\lambda_3}{2\sigma}\right)\right]. \quad (20)$$

These results should be easily extended to the distribution of shear eigenvalues at multiple points (e.g. Desjacques & Smith 2008).

2.6 Distribution of δ, e and p

In addition to the individual probability distributions of the three eigenvalues, we can also derive expressions for the quantities of most interest in the ellipsoidal collapse model. These are the ellipticity e and prolateness p, where

$$e = \frac{\lambda_1-\lambda_3}{2\delta}, \qquad \text{and} \qquad p = \frac{\lambda_1+\lambda_3-2\lambda_2}{2\delta} = \frac{1}{2}-\frac{3\lambda_2}{2\delta} = e-\frac{\lambda_2-\lambda_3}{\delta}. \quad (21)$$

The discussion above means that the distribution of e and p at fixed δ are unchanged from the Gaussian case:

$$g(e,\,p|\delta) = \frac{1125}{\sqrt{10\pi}}\,e\,(e^2-p^2)\left(\frac{\delta}{\sigma}\right)^5\,\mathrm{e}^{-(5/2)(\delta/\sigma)^2(3e^2+p^2)}. \quad (22)$$

However, the distribution of ellipticity is changed:

$$g(e) = \int \mathrm{d}p\int \mathrm{d}\delta\; g(e,\,p|\delta)\,p(\delta) \equiv g_0(e)+\frac{\sigma S_3}{6}\,\Delta g(e), \quad (23)$$

where

$$g_0(e) = \frac{45e}{\pi}\frac{1}{(1+20e^2)(1+15e^2)^{5/2}}\left[\sqrt{5}e\left(1+30e^2\right)\sqrt{1+15e^2}-\left(1+20e^2\right)\arctan\left(\frac{\sqrt{5}e}{\sqrt{1+15e^2}}\right)\right], \quad (24)$$

and

$$\Delta g(e) = \frac{-45000}{\sqrt{10\pi}}\frac{e}{|e|}\,e^4\left[\frac{4725e^6+90e^4-26e^2-1}{(1+15e^2)^4(1+20e^2)^{5/2}}\right]. \quad (25)$$

To check these expressions, we have used a Monte Carlo method to generate (x, y, z, Φ_{12}, Φ_{23}, Φ_{31}) (all but x are drawn from Gaussian distributions). We then solve the eigenvalue problem (by solving the associated cubic equation) to obtain (λ_1, λ_2, λ_3) and hence (δ_l, e, p). We then compute the distributions of the eigenvalues, and of δ, e and p, and compare them with the associated quantities when $f_{nl} = 0$. The symbols in Fig. 1 show our Monte Carlo results when the smoothing scale is $1\,h^{-1}$ Mpc, and the smooth curves show the analytic formulae derived above. Note the reflection symmetries in Figs 1 and 2 of the opposite sign of f_{nl}: it is due to that fact switching the sign of f_{nl} only changes the sign of $\sigma\ S_3/6$ without modifying other terms in $\Delta p(\lambda_i)$ and $\Delta g(e)$.

3 HALO ABUNDANCES

PS argued that the abundance of collapsed virialized haloes may be estimated from the statistics of the initial fluctuation field. They used the assumption that haloes form from a spherical collapse to argue that such objects started out as sufficiently overdense regions in the initial fluctuation field. They then used Gaussian statistics to estimate collapsed halo abundances. Although the way in which they used Gaussian statistics to make the estimate is flawed, LS suggested that one might be able to provide a better estimate of the abundance of collapsed haloes by repeating the PS argument, but changing the collapse model to allow halo formation to be non-spherical. In particular, they suggested that one should identify haloes with regions in the initial field where all three eigenvalues were greater than some critical value, λ_c. We will use the analysis above to show how this estimate of the halo mass function depends on f_{nl}.

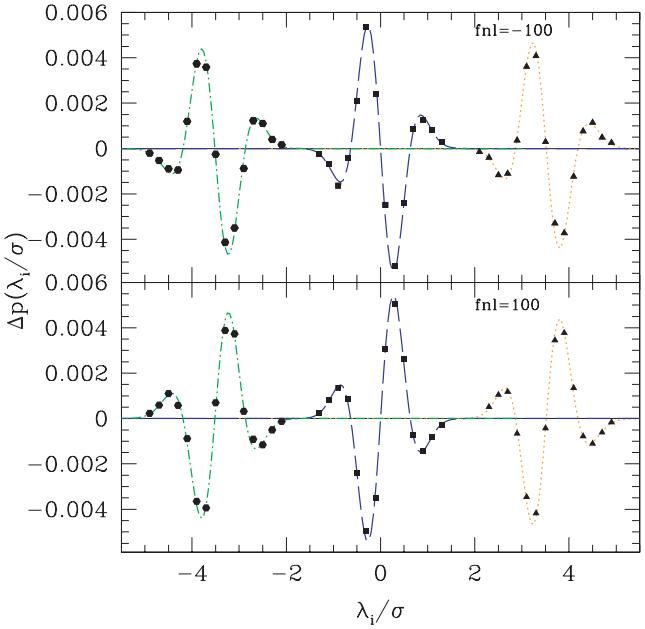

Figure 1. Difference between initial distributions in the f_{nl} and Gaussian models for $f_{nl} = 100$ (lower panels) and $f_{nl} = -100$ (upper panels) when the smoothing scale is $1\,h^{-1}$ Mpc. In both panels, the right and left plots show $p(\lambda_1/\sigma)$ (orange curve, triangle symbols) and $p(\lambda_3/\sigma)$ (green curve, hexagonal symbols), respectively. For clarity, these curves have been shifted to the right and to the left by 3. The middle plot shows $P(\lambda_2/\sigma)$ (blue curve, square symbols).

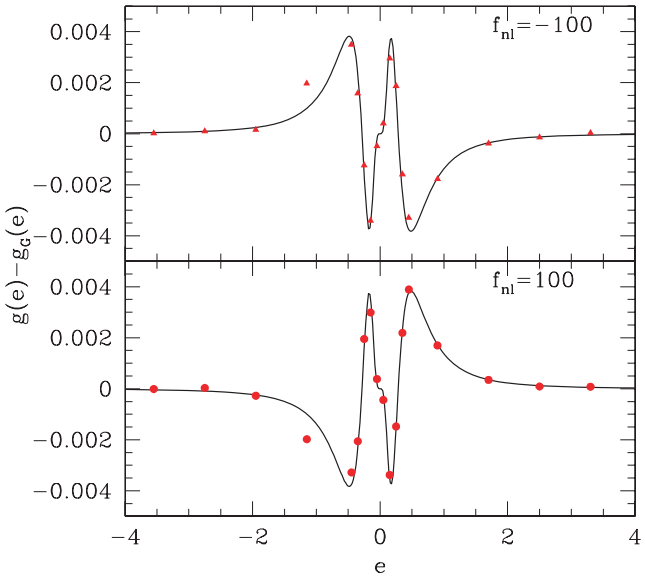

Figure 2. Difference between initial distributions of ellipticity e in the f_{nl} and Gaussian models for $f_{nl} = 100$ (lower panels) and $f_{nl} = -100$ (upper panels) when the smoothing scale is $1\,h^{-1}$ Mpc.

3.1 If halo formation depends on the initial overdensity exceeding a critical value

The PS-like estimate of the mass fraction in haloes above mass M is

$$F(>M) = F[<\sigma(R)] = \int_{\delta_c}^{\infty} \mathrm{d}\delta\, p(\delta|R) = \int_{\delta_c}^{\infty} \mathrm{d}\delta \left[1 + \frac{\sigma S_3}{6} H_3\right] p_0(\delta|R), \tag{26}$$

where $R = (3M/4\pi\bar{\rho})^{1/3}$, so $\sigma(R)$ is actually a function of M, and δ_c is the critical density required for collapse in the spherical model. So,

$$\frac{\partial F}{\partial \sigma} = \frac{\partial F_0}{\partial \sigma} + \frac{\partial(\sigma S_3/6)}{\partial \sigma}\left(\nu_c - \nu_c^{-1}\right)\nu_c\, p_0(\nu_c) - \frac{\sigma S_3}{6}\frac{\partial \ln \nu_c}{\partial \sigma}\nu_c\, p_0(\nu_c)\, H_3(\nu_c), \tag{27}$$

and hence

$$\frac{\partial F}{\partial \ln \nu_c} = \frac{\partial F_0}{\partial \ln \nu_c}\left[1 + \frac{\sigma S_3}{6}H_3(\nu_c) - \left(\nu_c - \nu_c^{-1}\right)\frac{\partial(\sigma S_3/6)}{\partial \ln \nu_c}\right] \approx \frac{\partial F_0}{\partial \ln \nu_c}\left[1 + \frac{\sigma S_3}{6}H_3(\nu_c)\right] \tag{28}$$

(Lo Verde et al. 2008); the term in brackets is the ratio of the halo mass function when $f_{nl} \neq 0$ to that when $f_{nl} = 0$ (Lam & Sheth 2009a, argue that, formally, the term in brackets is not the full story, but that it is, nevertheless, a good approximation.) The ratio $(\partial F/\partial \ln \nu_c)/(\partial F_0/\partial \ln \nu_c)$ provides a good description of the fractional change in the halo mass function induced by the coupling parameter f_{nl} (Desjacques et al. 2009), even though the functional form of $\partial F_0/\partial \ln \nu_c$ does not provide a good description of halo abundances in Gaussian cosmologies.

Halo abundances in $f_{nl} = 0$ simulations are usually well approximated by the functional form of Sheth & Tormen (1999):

$$\nu f(\nu) \equiv \frac{\partial F_0^{\rm ST}}{\partial \ln \nu} = 2A\sqrt{a}\,\nu\,\left[1 + (\sqrt{a}\,\nu)^{-2p}\right]\,\frac{{\rm e}^{-a\nu^2/2}}{\sqrt{2\pi}}, \tag{29}$$

where $p = 0.3,\ a = 0.7$ and $A = 0.322$ comes from requiring that the integral over all ν equal unity. Equation (26) with $f_{nl} = 0$ would yield $a = 1$ and $p = 0$, so A would be modified appropriately. Recently, Grossi et al. (2009) have studied the effect on the f_{nl} model of simply setting $\delta_c \to \sqrt{a}\delta_c$ in equation (26). In effect, they ignore the consequences of $p \neq 0$. However, Lam & Sheth (2009a) have shown that when the non-Gaussianity is weak, then the correction factor for halo abundances is well approximated by

$$\frac{\partial F/\partial \ln \nu_c}{\partial F_0/\partial \ln \nu_c} \approx 1 + \frac{\sigma S_3}{6} H_3\left(\frac{B(\sigma)}{\sigma}\right), \tag{30}$$

where

$$B(\sigma, z) = \sqrt{a}\,\delta_{\rm sc}(z)\,\left[1 + \beta(\sqrt{a}\,\delta_{\rm sc}/\sigma)^{-2\alpha}\right], \tag{31}$$

with $a = 0.7,\ \beta = 0.485$, *and* $\alpha = 0.615$, is motivated by models of triaxial collapse (Sheth et al. 2001; Sheth & Tormen 2002).

3.2 If halo formation depends on all three initial eigenvalues exceeding a critical value

Suppose that the criterion for halo formation is not that δ, the sum of the eigenvalues, exceeds δ_c, but that the smallest eigenvalue λ_3 exceeds λ_c. Then, the analogous argument yields

$$F(>M) = F[<\sigma(R)] = \int_{3\lambda_c}^{\infty} {\rm d}\delta\, p(\delta|R) \int_{\lambda_c}^{\delta/3} {\rm d}\lambda_3\, p(\lambda_3|\delta) = \int_{3\lambda_c}^{\infty} {\rm d}\delta\,\left[1 + \frac{\sigma S_3}{6} H_3\right]\, p_0(\delta|R)\, P_0(\lambda_3 > \lambda_c|\delta), \tag{32}$$

where

$$P_0(\lambda_3 \geq \lambda_c|\delta) = \left\{ -\frac{3\sqrt{10}}{4\sqrt{\pi}}\frac{(\delta - 3\lambda_c)}{\sigma}\exp\left[-\frac{5(\delta-3\lambda_c)^2}{8\sigma^2}\right] + \frac{1}{2}\left\{{\rm erf}\left[\frac{(\delta-3\lambda_c)\sqrt{10}}{4\sigma}\right] + {\rm erf}\left[\frac{(\delta-3\lambda_c)\sqrt{10}}{2\sigma}\right]\right\}\right\}\Theta(\delta - 3\lambda_c). \tag{33}$$

If we define $\ell_c \equiv \lambda_c/\sigma(R)$, then

$$F(\geq \ell_c) \equiv F_0(\geq \ell_c) + \frac{\sigma S_3}{6}\,\Delta F(\geq \ell_c), \qquad \text{where} \tag{34}$$

$$\begin{aligned}\Delta F(\geq \ell_c) &\equiv \int_{3\ell_c}^{\infty} {\rm d}\nu\,\frac{\exp(-\nu^2/2)}{\sqrt{2\pi}}\,\nu(\nu^2 - 3)\ P_0(\nu - 3\ell_c)\\ &= \frac{5^{3/2}}{162\sqrt{2\pi}}\left(100\ell_c^4 - 105\ell_c^2 + 9\right)\,\exp\left(-5\ell_c^2/2\right)\,{\rm erfc}(\sqrt{2}\ell_c) - \frac{5^{3/2}}{48\sqrt{3\pi}}\left(2 - 15\ell_c^2\right)\,\exp\left(-15\ell_c^2/4\right)\,{\rm erfc}(\sqrt{3}\ell_c/2)\\ &\quad + \frac{125\sqrt{5}}{648\pi}\,\ell_c\,\exp\left(-9\ell_c^2/2\right)\left(5 - 8\,\ell_c^2\right).\end{aligned} \tag{35}$$

The halo mass function is

$$\begin{aligned}\frac{\partial F}{\partial \ell_c} &= \frac{\partial F_0}{\partial \ell_c} + \frac{\partial(\sigma S_3/6)}{\partial \ell_c}\,\Delta F(\geq \ell_c) + \frac{\sigma S_3}{6}\frac{\partial(\Delta F)}{\partial \ell_c},\\ \frac{\partial F_0}{\partial \ell_c} &= -\frac{\sqrt{10}}{\sqrt{\pi}}\left(\frac{5\ell_c^2}{3} - \frac{1}{12}\right)\exp\left(-\frac{5\ell_c^2}{2}\right)\,{\rm erfc}(\sqrt{2}\ell_c) - \frac{\sqrt{15}}{4\sqrt{\pi}}\exp\left(-\frac{15\ell_c^2}{4}\right)\,{\rm erfc}\left(\frac{\sqrt{3}\ell_c}{2}\right) + \frac{5\sqrt{5}}{3\pi}\,\ell_c\,\exp\left(-\frac{9\ell_c^2}{2}\right),\\ \frac{\partial(\Delta F)}{\partial \ell_c} &= \frac{25}{2}\frac{\sqrt{5}}{2^4 3^4\pi}\left[\exp\left(-\frac{9\ell_c^2}{2}\right)\,\left(64 - 870\ell_c^2 + 800\ell_c^4\right) - \sqrt{2\pi}\,8\,\ell_c\left(51 - 185\ell_c^2 + 100\ell_c^4\right)\,\exp\left(-\frac{5\ell_c^2}{2}\right)\,{\rm erfc}(\sqrt{2}\ell_c)\right.\\ &\quad \left. + \sqrt{3\pi}\,3^4\ell_c\left(2 - 5\ell_c^2\right)\,\exp\left(-\frac{15\ell_c^2}{4}\right)\,{\rm erfc}\left(\frac{\sqrt{3}\ell_c}{2}\right)\right].\end{aligned} \tag{36}$$

Note that

$$\frac{\partial F}{\partial \ell_c} \neq \frac{\partial F_0}{\partial \ell_c}\,\left[1 + \frac{\sigma S_3}{6}\,H_3(\ell_c) - \left(\ell_c - \ell_c^{-1}\right)\frac{\partial(\sigma S_3/6)}{\partial \ln \ell_c}\right]. \tag{37}$$

Thus, in this case, the f_{nl} modification to the halo mass function is qualitatively different from that associated with the spherical evolution model.

We mentioned above that the ratio $(\partial F/\partial \ln \nu_c)/(\partial F_0/\partial \ln \nu_c)$ is well described by the term in brackets in equation (28). Since ν_c and ℓ_c are linearly proportional to one-another, it is interesting to ask if $(\partial F/\partial \ln \ell_c)/(\partial F_0/\partial \ln \ell_c)$ is also well described by the term in brackets

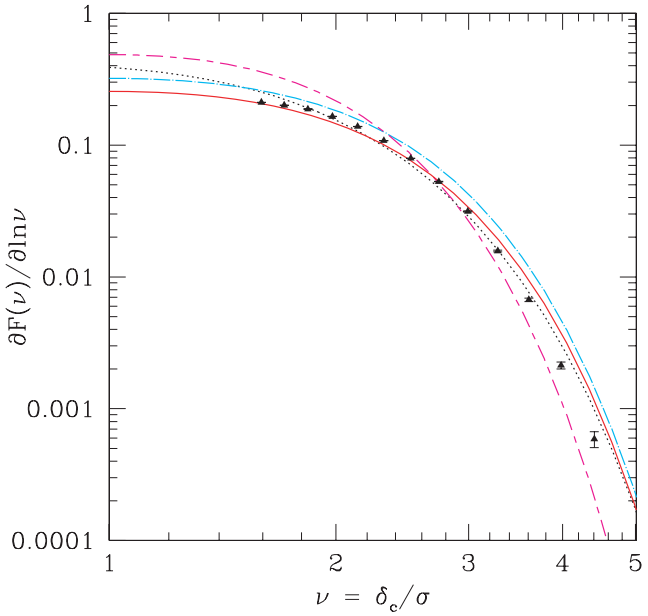

Figure 3. Halo multiplicity function $\partial F/\partial \ln \nu$ for the Gaussian simulations at $z = 0.3$. Black symbols show the measurements from simulations; short-long-dashed, dotted, dot-dashed and solid curves show equations (26), (36), (29) and (29) with a new normalization ($A = 0.26$), respectively.

in equation (28). (We have already shown that this ratio is not described by simply replacing $\nu_c \to 3\ell_c$.) Fig. 4 shows that it is not. Thus, if we were certain that the logic which leads to this estimate of the mass function were reliable, then we would conclude that, by studying how halo abundances depend on f_{nl}, we may have learnt something important about the physics of halo formation: the initial overdensity matters more than the value of the smallest eigenvalue.

3.3 Comparison with measurements from numerical simulations

Fig. 3 shows the multiplicity function measured in the $f_{nl} = 0$ simulations of Desjacques et al. (2009), where a detailed description of the runs can be found. (Our analysis is complementary to that of Pillepich et al. 2008, who have recently run a large set of simulations of the f_{nl} model; they studied halo abundances *and* clustering in their simulations.) Curves show equation (26) (magenta, short-long-dashed), equation (36) (black, dotted) and equation (29) (cyan, dashed) with $\delta_c = 1.66$ and $\lambda_c = 0.41$. In contrast to most previous works, equation (36) appears to give a better fit than equation (29); this may be due to the fact that the halo finder (AHF, see Knollmann & Knebe 2009) is not standard. (The halo-finder used by Pillepich et al. 2008 is more standard, and they indeed find that equation 29, with standard choices for its free parameters, works well.) The red solid curve shows equation (29) with a new normalization ($A = 0.26$) and the agreement with the numerical measurements is much better.

It is conventional to show the effects of $f_{nl} \neq 0$ on the mass function by ratioing with respect to the $f_{nl} = 0$ case. The symbols in Fig. 4 show this ratio for $f_{nl} = 100$ (left-hand panel) and -100 (right-hand panel), respectively. The short-long-dashed, dotted and dot-dashed curves show these ratios for the same models as in the previous figure (equations 28, 36 and A1). The solid (red) curve shows equation (30). The estimate motivated by the spherical collapse model (equation 28) describes the measured ratio very well (in agreement with Lo Verde et al. 2008; Desjacques et al. 2009; Grossi et al. 2009), even though the mass function on which it is based is a bad fit to the $f_{nl} = 0$ data. On the other hand, the same logic applied to a prescription based on the smallest eigenvalue (equation 36) fits the Gaussian (i.e. $f_{nl} = 0$) mass function reasonably well, but does not describe deviations from non-Gaussianity very well! In addition, the same logic applied to the Sheth & Tormen (1999) mass function (equation A1) also does not fit the ratio very well. However, our excursion set based approach (equation 30) seems to match the measurement as well as, if not better than, any of the other methods. Note that it is the only model which matches both the $f_{nl} = 0$ mass function, *and* the $f_{nl} \neq 0$ ratio. We also checked that our excursion set based approach agrees with Pillepich et al. (2008) fitting formula's prediction (less than 6 per cent difference in the range of validity of the fitting formula, which is $1.4 < \nu < 5$).

4 VOID ABUNDANCES

Underdense regions are also a good probe of f_{nl} (Lam & Sheth 2009b). Kamionkowski et al. (2009) have applied the analogue of equation (26) to study void abundances when $f_{nl} \neq 0$. In what follows, we estimate void abundances associated with the analogue of Section 3.2 by assuming they are simply the opposite of haloes. However, because of the 'void-in-cloud' problem identified by Sheth & van de Weygaert (2004), even when $f_{nl} = 0$, these analyses are, at best, appropriate only for the largest voids. Hence, we also discuss the effect of including the correction for the 'void-in-cloud' problem.

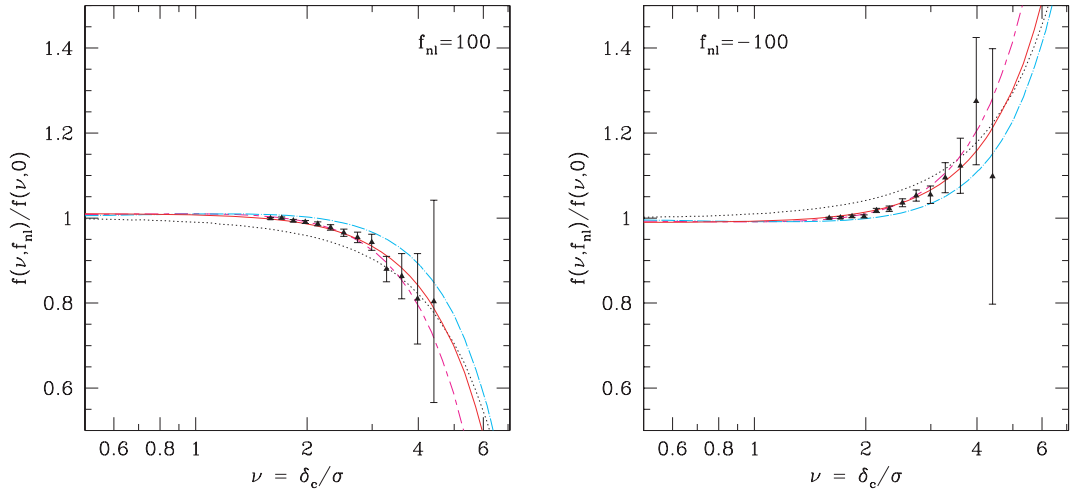

Figure 4. The ratio of halo mass function of $f_{nl} = 100$ models to the corresponding Gaussian models using equations (28), (30), (A1) and (36), (magenta short-long-dashed, solid red, cyan dot-dashed and black dotted). Panel on left shows $f_{nl} = 100$ and panel on the right shows $f_{nl} = -100$.

4.1 If voids formation depends on all three eigenvalues lying below a critical value

Given a critical value λ_v, the corresponding mass function of voids is

$$F(<M) = \int_{-\infty}^{3\lambda_v} \mathrm{d}\delta\, p(\delta|R) \int_{\delta/3}^{\lambda_v} \mathrm{d}\lambda_1\, p(\lambda_1|\delta) = \int_{-\infty}^{3\lambda_v} \mathrm{d}\delta \left[1 + \frac{\sigma S_3}{6} H_3\right] p_0(\delta|R) P_0(\lambda_1 < \lambda_v|\delta), \tag{38}$$

where

$$P_0(\lambda_1 \le \lambda_v|\delta) = \left\{ -\frac{3\sqrt{10}}{4\sqrt{\pi}} \frac{(3\lambda_v - \delta)}{\sigma} \exp\left[-\frac{5(3\lambda_v-\delta)^2}{8\sigma^2}\right] + \frac{1}{2}\left\{ \mathrm{erf}\left[\frac{(3\lambda_v-\delta)\sqrt{10}}{4\sigma}\right] \mathrm{erf}\left[\frac{(3\lambda_v-\delta)\sqrt{10}}{2\sigma}\right]\right\}\right\} \Theta(3\lambda_v - \delta). \tag{39}$$

If we define $\ell_v \equiv \lambda_v/\sigma$, then the corresponding $F_0(\le \ell_v)$ and $\Delta\, F(\le \ell_v)$ can be obtained by replacing erfc (x) by $-[1 + \mathrm{erf}\,(x)]$ in equations (34) and (35). The void mass function can be obtained by making the same replacement, so it is

$$\begin{aligned}
\frac{\partial F}{\partial \ell_v} &= \frac{\partial F_0}{\partial \ell_v} + \frac{\partial(\sigma S_3/6)}{\partial \ell_v} \Delta F(\le \ell_v) + \frac{\sigma S_3}{6} \frac{\partial(\Delta F)}{\partial \ell_v}, \\
\frac{\partial F_0}{\partial \ell_v} &= \frac{\sqrt{10}}{\sqrt{\pi}} \left(\frac{5\ell_v^2}{3} - \frac{1}{12}\right) \exp\left(-\frac{5\ell_v^2}{2}\right) \left[1 + \mathrm{erf}(\sqrt{2}\ell_v)\right] + \frac{\sqrt{15}}{4\sqrt{\pi}} \exp\left(-\frac{15\ell_v^2}{4}\right) \left[1 + \mathrm{erf}\left(\frac{\sqrt{3}\ell_v}{2}\right)\right] + \frac{5\sqrt{5}}{3\pi} \ell_v \exp\left(-\frac{9\ell_v^2}{2}\right). \\
\frac{\partial(\Delta F)}{\partial \ell_v} &= \frac{25}{2} \frac{\sqrt{5}}{2^4 3^4 \pi} \left\{ \exp\left(-\frac{9\ell_v^2}{2}\right) \left(64 - 870\ell_v^2 + 800\ell_v^4\right) + \sqrt{2\pi} 8\ell_v \left(51 - 185\ell_v^2 + 100\ell_v^4\right) \exp\left(-\frac{5\ell_v^2}{2}\right) \left[1 + \mathrm{erf}(\sqrt{2}\ell_v)\right] \right. \\
&\quad \left. - \sqrt{3\pi} 3^4 \ell_v \left(2 - 5\ell_v^2\right) \exp\left(-\frac{15\ell_v^2}{4}\right) \left[1 + \mathrm{erf}\left(\frac{\sqrt{3}\ell_v}{2}\right)\right]\right\}.
\end{aligned} \tag{40}$$

4.2 Void-in-cloud problem: excursion set approach

An important aspect in the void abundance is the overcounting of the voids located inside collapsing regions. The formalism of counting voids as regions below some critical value [denoted δ_v in Kamionkowski et al. (2009) and λ_v in the discussion above] does not account for this. Sheth & van de Weygaert (2004) examined this problem using the excursion set approach by studying a two barriers problem: δ_c for haloes and δ_v for voids.

We will now extend the calculation of the void-in-cloud effect to models where $f_{nl} \neq 0$. We use the constant barriers to demonstrate the method. Denote the two constant barriers correspond to the formation of haloes and voids by δ_c and δ_v, $\mathcal{F}(s, \delta_v, \delta_c)$ as the probability of a random walk crossing the barrier δ_v at scale s and it did not cross the other barrier δ_c. This probability is directly connected to the void abundances, including the void-in-cloud effect, as the random walk never crossed the halo formation barrier. It is related to the first crossing distribution $f(s, \delta_v)$ by

$$\mathcal{F}(s, \delta_v, \delta_c) = f(s, \delta_v) - \int_0^s \mathrm{d}S_1\, \mathcal{F}(S_1, \delta_c, \delta_v) f(s, \delta_v|S_1, \delta_c), \tag{41}$$

where the second term on the right-hand side substracts from the first crossing those walks that crossed δ_c at S_1 before crossing δ_v at s (but never had crossed δ_v before S_1). Swaping δ_v and δ_c:

$$\mathcal{F}(S_1, \delta_c, \delta_v) = f(S_1, \delta_c) - \int_0^{S_1} \mathrm{d}S_2\, \mathcal{F}(S_2, \delta_v, \delta_c) f(S_1, \delta_c|S_2, \delta_v). \tag{42}$$

Substituting equation (42) into equation (41), we find

$$\mathcal{F}(s,\delta_{\rm v},\delta_{\rm c}) = f(s,\delta_{\rm v}) - \int_0^s {\rm d}S_1\, f(s,\delta_{\rm v}|S_1,\delta_{\rm c}) f(S_1,\delta_{\rm c}) + \int_0^s {\rm d}S_1 \int_0^{S_1} {\rm d}S_2 f(s,\delta_{\rm v}|S_1,\delta_{\rm c}) f(S_1,\delta_{\rm c}|S_2,\delta_{\rm v}) \mathcal{F}(S_2,\delta_{\rm v},\delta_{\rm c}) \tag{43}$$

$$= f(s,\delta_{\rm v}) + \sum_{n=1}^{\infty}(-1)^n \int_0^{S_0} {\rm d}S_1, \ldots, \int_0^{S_{n-1}} {\rm d}S_n \prod_{m=0}^{n-1} f(S_m,\delta_m|S_{m+1},\delta_{m+1}) f(S_n,\delta_n), \tag{44}$$

where the last expression is obtained after inserting equations (41) and (42) successively. Furthermore, $S_0 \equiv s$ and

$$\delta_n = \begin{cases} \delta_{\rm v} & \text{if } n \text{ is even} \\ \delta_{\rm c} & \text{if } n \text{ is odd.} \end{cases} \tag{45}$$

The nth order term in the summation of equation (44) denotes walks that have crossed the two barriers alternatively n times before crossing $\delta_{\rm v}$ at s. Below we will work out the predictions of equation (44) for primordial Gaussian perturbations and for models with primordial non-Gaussianity of the f_{nl} type.

4.2.1 Gaussian initial conditions

We would like to estimate $f(s,\delta_{\rm v}|S,\delta_{\rm c})$, which is the first crossing probability of $\delta_{\rm v}$ at scale s given it crossed the barrier $\delta_{\rm c}$ at some scale S ($< s$). For Gaussian distributions with sharp-k space filters, $f_0(s,\delta_{\rm v}|S,\delta_{\rm c}) = f_0(s-S,\delta_{\rm v}-\delta_{\rm c})$, and equation (44) reduces to

$$\begin{aligned}\mathcal{F}_0(s,\delta_{\rm v},\delta_{\rm c}) &= f_0(s,\delta_{\rm v}) + \sum_{n=1}^{\infty}(-1)^n \int_0^{S_0} {\rm d}S_1, \ldots, \int_0^{S_{n-1}} {\rm d}S_n \left[\prod_{m=0}^{n-1} f_0(S_m,\delta_m|S_{m+1},\delta_{m+1})\right] f_0(S_n,\delta_n), \\ &\approx f_0(s,\delta_{\rm v}) \exp\left(-\frac{|\delta_{\rm v}|}{\delta_{\rm c}}\frac{\mathcal{D}^2}{4\nu^2} - 2\frac{\mathcal{D}^4}{\nu^4}\right),\end{aligned} \tag{46}$$

where the last expression is the approximation given by Sheth & van de Weygaert (2004) with $\mathcal{D} \equiv |\delta_{\rm v}|/(\delta_{\rm c}+|\delta_{\rm v}|)$ and $\nu \equiv \delta_{\rm v}/\sqrt{s}$.

4.2.2 Local non-Gaussian f_{nl} models

The calculation of the conditional first crossing probability $f(\delta_{\rm v}, s|\delta_{\rm c}, S)$ for the f_{nl} model is analogous to that of halo abundances (Lam & Sheth 2009a). First, we write down the probability $p(s,\delta|S,\delta_{\rm v})$ as

$$p(s,\delta|S,\delta_{\rm c}) = \int_S^s {\rm d}S'\, f(S',\delta_{\rm v}|S,\delta_{\rm c})\, p(s,\delta|S',\delta_{\rm v}|S,\delta_{\rm c}), \tag{47}$$

provided that $\delta < \delta_{\rm v}$. So,

$$P(s,\delta_{\rm v}|S,\delta_{\rm c}) \equiv \int_{-\infty}^{\delta_{\rm v}} {\rm d}\delta\, p(s,\delta|S,\delta_{\rm c}) = \int_S^s {\rm d}S'\, f(S',\delta_{\rm v}|S,\delta_{\rm c}) \int_{-\infty}^{\delta_{\rm v}} {\rm d}\delta\, p(s,\delta|S',\delta_{\rm v}|S,\delta_{\rm c}). \tag{48}$$

The derivative with respect to s is

$$\frac{\partial P(s,\delta_{\rm v}|S,\delta_{\rm c})}{\partial s} = \frac{f(s,\delta_{\rm v}|S,\delta_{\rm c})}{2} + \int_S^s {\rm d}S'\, f(S',\delta_{\rm v}|S,\delta_{\rm c}) \frac{\partial}{\partial s}\int_{-\infty}^{\delta_{\rm v}} {\rm d}\delta\, p(s,\delta|S',\delta_{\rm v}|S,\delta_{\rm c}). \tag{49}$$

The above equation is an integral equation for $f(\delta_{\rm v}, s|\delta_{\rm c}, S)$ and its zeroth-order solution is given by the left-hand side of the equation (which can be evaluated using the bivariate Edgeworth expansion). We argue that, in analogy to the calculation of the halo abundance, the first-order solution is negligible compared to the zeroth order. Therefore, we can make the following approximation:

$$f(s,\delta_{\rm v}|S,\delta_{\rm c}) \approx 2\frac{\partial P(s,\delta_{\rm v}|S,\delta_{\rm c})}{\partial s}. \tag{50}$$

Note that for Gaussian distributions,

$$\begin{aligned}\frac{\partial P_0(s,\delta_{\rm v}|S,\delta_{\rm c})}{\partial s} &= \frac{\partial}{\partial s}\int_{-\infty}^{(\delta_{\rm v}-\delta_{\rm c})/\sqrt{s-S}} {\rm d}x\, \frac{{\rm e}^{-x^2/2}}{\sqrt{2\pi}}, \\ &= \frac{-(\delta_{\rm v}-\delta_{\rm c})}{2(s-S)}\frac{\exp[-(\delta_{\rm v}-\delta_{\rm c})^2/2(s-S)]}{\sqrt{2\pi(s-S)}},\end{aligned} \tag{51}$$

which is the expected conditional distribution for Gaussian statistics.

In Appendix B, the right-hand side of equation (50) is evaluated using the Edgeworth expansion. Here, we will approximate the conditional first crossing probability by

$$f(s,\delta_{\rm v}|S,\delta_{\rm c}) \approx f_0(s,\delta_{\rm v}|S,\delta_{\rm c})\left[1 + \frac{\sigma S_3}{6}\,\zeta(s,\delta_{\rm v},S,\delta_{\rm c})\right], \tag{52}$$

where

$$\zeta(s,\delta_{\rm v},S,\delta_{\rm c}) = -2\frac{\partial\mathcal{E}(s,S)}{\partial s}\frac{(s-S)^{3/2}}{|\delta_{\rm v}-\delta_{\rm c}|} - \mathcal{E}(s,S)\frac{|\delta_{\rm v}-\delta_{\rm c}|}{\sqrt{s-S}}. \tag{53}$$

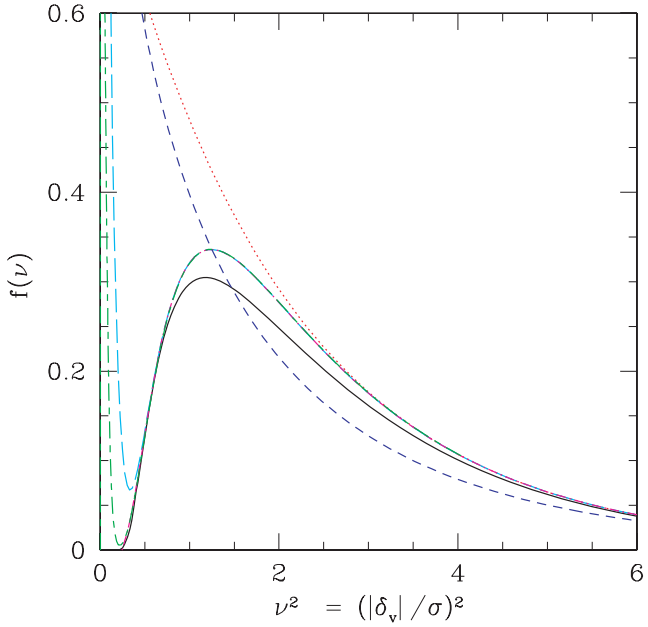

Figure 5. Predicted void abundances for Gaussian initial conditions. Solid (black) curve shows equation (46) with $(\delta_v, \delta_c) = (-2.81, 1.66)$. Long-dashed (cyan), dot-dashed (magenta) and short-long-dashed (green) curves are the solution to equation (44) with $n = 2, 3, 4$, respectively. Predictions without the void-in-cloud effect are also shown: dotted (red) is the zeroth order solution of equation (44), which is equivalent to the PS result; short-dashed (blue) shows the prediction from the LS formalism (equation 40 with $\lambda_v = -0.69$).

Substituting equation (52) into equation (44) and keeping only terms linear in $(\sigma\ S_3/6)$, we can recast the integral equation into the form

$$\mathcal{F}(s,\delta_v,\delta_c) = \mathcal{F}_0(s,\delta_v,\delta_c) + \frac{\sigma S_3}{6}\Bigg\{ f_0(s,\delta_v) H_3\left(\frac{\delta_v}{\sqrt{s}}\right) + \sum_{n=1}^{\infty}(-1)^n \int_0^{S_0} \mathrm{d}S_1, \ldots, \int_0^{S_{n-1}} \mathrm{d}S_n \left[\prod_{m=0}^{n-1} f_0(S_m,\delta_m|S_{m+1},\delta_{m+1})\right] f_0(S_n,\delta_n)\left[\sum_{m=0}^{n-1}\zeta(S_m,\delta_m,S_{m+1},\delta_{m+1}) + H_3\left(\frac{\delta_n}{\sqrt{S_n}}\right)\right]\Bigg\}. \tag{54}$$

4.3 Comparison of models

Fig. 5 shows theoretical expectations of void abundances when $f_{nl} = 0$: the solid (black) curve shows equation (46) with $(\delta_v, \delta_c) = (-2.81, 1.66)$. The long-dashed (cyan), dot-dashed (magenta) and short-long-dashed (green) curves show equation (44), keeping terms up to $n = 2, 3, 4$, respectively. The zeroth order solution of equation (44) without the void-in-cloud effect is shown as the dotted (red) curve. It is the first crossing probability of a constant barrier and is the same as the PS prediction. Finally, the short-dashed (blue) shows the prediction of the LS formalism (equation 40) with $\lambda_v = -0.69$.

The predictions from the PS formalism and the LS formalism (both without the void-in-cloud effect) are different over a large range of void size, so comparisons with numerical measurements could distinguish which models describe best the formation of voids. Furthermore, while the effect of void-in-cloud is significant for small voids, it is negligible for big voids.

The approximation equation (46) provides a very good description of the solution to the integral equation (44), even in the regime of very small voids ($\nu^2 \sim 0.5$) for which equation (44) requires the inclusion of high order terms. If one characterizes the accuracy of the n-order term by the smallest ν at which the inclusion of the next order term modifies the result by less than 1 per cent, then the second and third orders are accurate for $\nu \gtrsim 0.9$ and $\gtrsim 0.6$.

Fig. 6 compares the ratio of the void abundances for $f_{nl} \neq 0$ relative to the case $f_{nl} = 0$ for the various analytic approximations described above. The curve labels are identical to those in the previous figures, except for the solid (black) curve showing equation (28) and an addition dot-long-dashed (orange) curve showing the same equation upon neglecting the $\partial(\sigma S_3)/\partial s$ term. These two curves, as well as the short-dashed (blue) curve, include the scale dependence of σS_3 using the approximation formula given in Lam & Sheth (2009a). The other curves [dotted (red), long-dashed (cyan), dot-short-dashed (magenta) and short-long-dashed (green) for $n = 0, 2, 3, 4$ in equation 44] assume a constant $\sigma S_3 = 0.022$. As we can see, unlike halo abundances, a positive value of f_{nl} increases the relative number of big voids, whereas a negative f_{nl} decreases it.

The overlapping of the solid (black), dot-long-dashed (orange) and dotted (red) curves justifies a posteriori our assumption of constant σS_3. For big voids, the dotted curve deviates only slightly from the other two where it agrees reasonably well with higher order solutions to the integral equation (44). Hence, the difference between the various curves (apart from the blue short-dashed) are mostly governed by

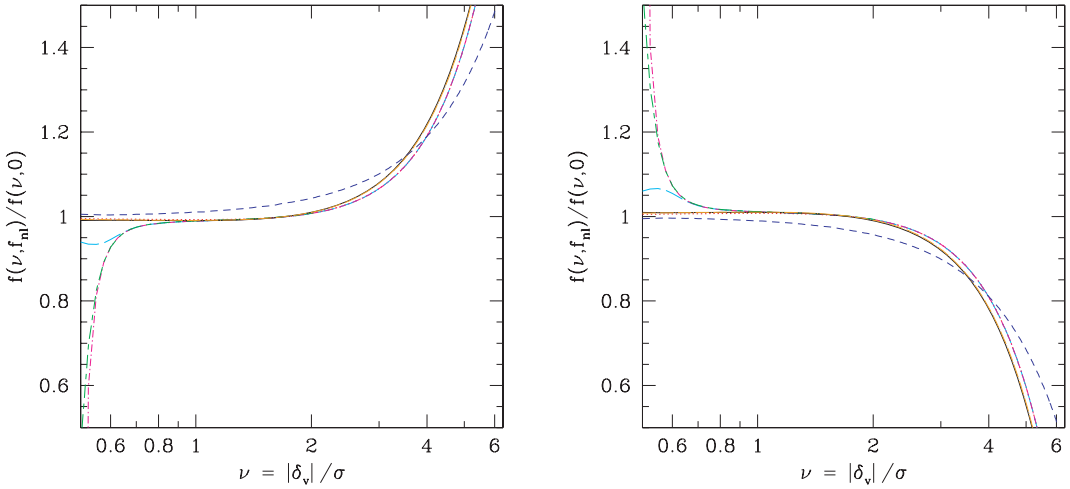

Figure 6. Ratio of void abundances of $f_{nl} \neq 0$ to the $f_{nl} = 0$ case. Left- and right-hand panels show $f_{nl} = 100$ and -100, respectively. Curve labels are the same as the previous figure, with the exception of the solid (black) showing the PS prediction (the square brackets in equation 28) and an addition dot-long-dashed (orange) curve showing the same equation but ignoring the $\partial(\sigma S_3)/\partial s$ term. Models without the void-in-cloud effect (black solid, blue short-dashed and orange dot-long-dashed) include the scale dependence of σS_3; the others use $|\sigma S_3| = 0.022$.

σS_3 rather than the different functional form of the models. Note, however, that the prediction of the LS formalism (blue short-dashed) considerably departs from the other curves.

Including higher order terms in equation (44) so as to better account for the void-in-cloud effect does not change the results for big voids. This is expected from our model in which big voids are unlikely to be embedded in a larger collapsing region. However, including the void-in-cloud effect modifies the ratio of void abundances for the smallest voids. Namely, a positive f_{nl} tend to decrease the number of small voids. This may originate from an increase of high-mass haloes, which is such that small voids are more likely to sit inside an collapsing region. Our prediction is at best qualitative because higher order terms are needed to describe accurately the small voids regime [Our results shown in Fig. 5 indicate that the third order approximation (magenta) is valid only for $\nu \gtrsim 0.6$]. We have not pursued the inclusion of higher order corrections here since constant barriers may not be a good approximation for the formation of haloes and voids as suggested by the analysis of (Gaussian) initial conditions of cosmological simulations. None the less, our formalism allows the incorporation of scale dependence barriers, which shall be useful when numerical measurements are available.

5 DISCUSSION

We extended the Doroshkevich's celebrated formulae for the eigenvalues of the initial shear field associated with Gaussian statistics to the local non-Gaussian f_{nl} model. We showed that, up to second order in f_{nl}, this is straightforward because, at fixed overdensity, the distribution is the same as when $f_{nl} = 0$ (i.e. Gaussian initial conditions). Our analytic formulae are in good agreement with measurements of the distribution of $(\lambda_1, \lambda_2, \lambda_3)$ in Monte Carlo realizations of the f_{nl} distribution (Figs 1 and 2).

Our extension of the Doroshkevich's formulae to the local non-Gaussian f_{nl} model provides the first step in the study of triaxial structure formation in models with primordial non-Gaussianity. This is interesting because, for Gaussian initial conditions, halo formation is more triaxial than spherical. In particular, in the triaxial collapse model, the evolution of a patch depends on its initial overdensity δ as well as the parameters e and p, which describe its initial ellipticity and prolateness. We showed that the distribution of e and p at fixed δ is unchanged from when $f_{nl} = 0$ (equation 22). Therefore, equation (31), which was determined for $f_{nl} = 0$ models, should continue to be useful even when $f_{nl} \neq 0$.

We applied our formulae for the initial shear field to study the change in halo and void abundances in the local non-Gaussian model (Section 3). When $f_{nl} = 0$, halo abundances predicted by a model in which halo formation is associated with having all three initial shear eigenvalues above some critical value are in better agreement with the simulations than those implied by the usual overdensity threshold criterion (Fig. 3). However, the predicted dependence of $f(\nu, f_{nl})/f(\nu, 0)$ f_{nl} is in better agreement with the simulations (see Fig. 4) in the latter case.

To understand this better, we extended the ellipsoidal collapse formalism to the local non-Gaussian model. We included the moving barrier formulation of ellipsoidal collapse (Sheth et al. 2001; Sheth & Tormen 2002) using two different approaches. The first is analogous to that used in the case of spherical collapse (Section A); the predicted dependence on f_{nl} did not agree with measurements from the simulations. The second is an extension of the excursion set approach following Lam & Sheth (2009a). For the case of a constant barrier (associated with spherical collapse), this approach reproduces the results of Lo Verde et al. (2008) and Maggiore & Riotto (2009b). Its extension to moving barriers appears promising since it matches the measured halo counts when $f_{nl} = 0$ as well as the dependence on f_{nl} (Fig. 4).

For f_{nl} models, differences in the density field evolved from Gaussian and non-Gaussian initial conditions are more dramatic in the underdense regions (Lam & Sheth 2009b). Fig. 5 shows a number of predictions for void abundances for $f_{nl} = 0$, while Fig. 6 shows the effect

of using our triaxial formalism to study how these depend on f_{nl}. The trends are generally like those in the halo abundance, except that the dependence on the sign of f_{nl} is reversed (compare Figs 4 and 6). This is consistent with the recent work of Kamionkowski et al. (2009). Still, one might have expected that an excess of massive haloes also implies an excess of large voids (since all the mass is concentrated in a smaller volume). This is what is indeed found for $f_{nl} = 0$ when one increases the normalization amplitude σ_8 of the fluctuation field. However, this is not true in f_{nl} models. In this respect, void abundances provide complementary information to cluster abundances, so a joint comparison of both could be used to put constraints on the level of non-Gaussianity.

We also demonstrated how the void-in-cloud effect can be included in models where $f_{nl} \neq 0$. We used the constant barriers as an example. We found that the inclusion of the void-in-cloud effect modifies the abundances of small voids. As a result, models with positive f_{nl} show a strong decrement in very small voids whereas models with negative f_{nl} show the opposite. This may be due to the enhancement of high-mass haloes for $f_{nl} > 0$ which effectively increases the probability of finding small voids inside a high-mass halo. Higher order terms in equation (44) and a more accurate description of scale dependent barriers will be needed to make more quantitative predictions.

Our results have other applications which we have not completed. The distribution of the eigenvalues of the initial shear field can be used to study the shapes of haloes and voids; combining the signals with the halo/void abundance and shape distribution would further constrain the value of f_{nl}. This is a subtle point because, although halo shapes are expected to correlate with the parameters e and p, we have shown that, at fixed δ, the distribution of e and p does not depend on f_{nl}. Hence, naively, the shape distribution is not informative. In practice, one usually averages over a range of halo masses. In other words, these will have a range of δ/σ values, so the result of this averaging may depend on f_{nl}, for the same reason that the distribution of e (equation 23) depends on f_{nl}. And finally, we are in the process of extending our non-linear redshift space probability distribution function for the dark matter (Lam & Sheth 2008) to these f_{nl} models.

ACKNOWLEDGMENTS

We would like to thank the referee for a helpful report. VD acknowledges support by the Swiss National Foundation under contract No. 200021-116696/1.

REFERENCES

Afshordi N., Tolley A. J., 2008, Phys. Rev. D, 78, 123507
Bardeen J. M., Bond J. R., Kaiser N., Szalay A. S., 1986, ApJ, 304, 15
Bernardeau F., Colombi S., Gaztañaga E., Scoccimarro R., 2002, Phys. Rep., 367, 1
Bond J. R., Myers S. T., 1996, ApJS, 103, 1
Bond J. R., Cole S., Efstathiou G., Kaiser N., 1991, ApJ, 379, 440
Buchbinder E. I., Khoury J., Ovrut B. A., 2008, Phys. Rev. Lett., 100, 171302
Carbone C., Verde L., Matarrese S., 2008, ApJ, 684, L1
Dalal N., Doré O., Huterer D., Shirokov A., 2008, Phys. Rev. D, 77, 123514
Desjacques V., 2008, MNRAS, 388, 638
Desjacques V., Smith R. E., 2008, Phys. Rev. D, 78, 023527
Desjacques V., Seljak U., Iliev I. T., 2009, MNRAS, 396, 85
Doroshkevich A. G., 1970, Astrofizika, 6, 581
Grossi M., Branchini E., Dolag K., Matarrese S., Moscardini L., 2008, MNRAS, 390, 438
Grossi M., Verde L., Carbone C., Dolag K., Branchini E., Iannuzzi F., Matarrese S., Moscardini L., 2009, preprint (arXiv:902.2013)
Hikage C., Matsubara T., Coles P., Liguori M., Hansen F. K., Matarrese S., 2008, MNRAS, 389, 1439
Izumi K., Soda J., 2007, Phys. Rev. D, 76, 083517
Kamionkowski M., Verde L., Jimenez R., 2009, J. Cosmology Astroparticle Phys., 1, 10
Khoury J., Piazza F., 2009, J. Cosmology Astroparticle Phys., 07, 026
Knollmann S. R., Knebe A., 2009, ApJS, 182, 608
Komatsu E. et al., 2009, ApJS, 180, 330
Koyama K., Soda J., Taruya A., 1999, MNRAS, 310, 1111
Lam T. Y., Sheth R. K., 2008, MNRAS, 389, 1249
Lam T. Y., Sheth R. K., 2009a, preprint (arXiv:0905.1702)
Lam T. Y., Sheth R. K., 2009b, MNRAS, 395, 1743
Lee J., Shandarin S. F., 1998, ApJ, 500, 14 (LS)
Lo Verde M., Miller A., Shandera S., Verde L., 2008, J. Cosmology Astroparticle Phys., 4, 14
Maggiore M., Riotto A., 2009a, preprint (arXiv:0903.1250)
Maggiore M., Riotto A., 2009b, preprint (arXiv:0903.1251)
Maldacena J., 2003, J. High Energy Phys., 5, 13
Matarrese S., Verde L., 2008, ApJ, 677, L77
Matarrese S., Verde L., Jimenez R., 2000, ApJ, 541, 10
McDonald P., 2008, Phys. Rev. D, 78, 123519
McEwen J. D., Hobson M. P., Lasenby A. N., Mortlock D. J., 2008, MNRAS, 388, 659
Pillepich A., Porciani C., Hahn O., 2008, preprint (arXiv:0811.4176)
Press W. H., Schechter P., 1974, ApJ, 187, 425 (PS)
Rossi G., Sheth R. K., Park C., Hernandez-Monteagudo C., 2009, preprint (arXiv:0906.2190)
Scoccimarro R., Sefusatti E., Zaldarriaga M., 2004, Phys. Rev. D, 69, 103513

Sefusatti E., Komatsu E., 2007, Phys. Rev. D, 76, 083004
Sheth R. K., Tormen G., 1999, MNRAS, 308, 119
Sheth R. K., Tormen G., 2002, MNRAS, 329, 61
Sheth R. K., van de Weygaert R., 2004, MNRAS, 350, 517
Sheth R. K., Mo H. J., Tormen G., 2001, MNRAS, 323, 1
Silvestri A., Trodden M., 2008, preprint (arXiv:0811.2176)
Slosar A., 2009, J. Cosmology Astroparticle Phys., 3, 4
Slosar A., Hirata C., Seljak U., Ho S., Padmanabhan N., 2008, J. Cosmology Astroparticle Phys., 8, 31
Taruya A., Koyama K., Matsubara T., 2008, Phys. Rev. D, 78, 123534
Yadav A. P. S., Wandelt B. D., 2008, Phys. Rev. Lett., 100, 181301
Zel'Dovich Y. B., 1970, A&A, 5, 84

APPENDIX A: CRITICAL VALUE APPROACH

The derivation of equation (26), which assumes that F is simply related to P, without writing the intermediate steps associated with the excursion set approach, is ad hoc. For example, if we assume the same logic that leads to equation (26) but choose the integrand $p(\delta|R)$ so that it returns equation (29) in the case $f_{nl} = 0$, then we find that

$$\nu_{\rm c} f(\nu_{\rm c}) \equiv \frac{\partial F}{\partial \ln \nu_{\rm c}} = \frac{\partial}{\partial \ln \nu_{\rm c}} \int_{\sqrt{a}\,\nu_{\rm c}}^{\infty} {\rm d}\nu\, 2A \left[1 + \frac{\sigma S_3}{6} H_3\right] \left(1 + \frac{1}{\nu^{2p}}\right) \frac{{\rm e}^{-\nu^2/2}}{\sqrt{2\pi}},$$
$$= \frac{\partial\, F_0^{\rm ST}}{\partial \ln \nu_{\rm c}} \left(1 + \frac{\sigma S_3}{6} H_3(\sqrt{a}\,\nu_{\rm c})\right) + \frac{\partial(\sigma S_3/6)}{\partial \ln \nu_{\rm c}} \frac{2A}{\sqrt{2\pi}} \left\{ {\rm e}^{-a\nu_{\rm c}^2/2} \left[a\nu_{\rm c}^2 - 1 + \left(a\nu_{\rm c}^2\right)^{1-p} \right] - \frac{1+2p}{2^p}\, \Gamma\left(1-p, \frac{a\nu_{\rm c}^2}{2}\right) . \right\}. \quad \text{(A1)}$$

The first line of this expression has not made its way into the $f_{nl} = 0$ literature – a testament to how much more popular the excursion set approach (see below) has become. It does not provide a particularly good description of the measured dependence on f_{nl}, so we do not consider it further.

APPENDIX B: BIVARIATE EDGEWORTH EXPANSION FOR VOID ABUNDANCES

We used the bivariate Edgeworth expansion to study the first crossing probability when $f_{nl} \neq 0$ in Lam & Sheth (2009a). We can define the analogy of $\mathcal{G}_{mn}$ here:

$$Q_{mn} = \int_{-\infty}^{0} {\rm d}\delta\; p_0(\delta + \delta_{\rm v}, s|\delta_{\rm c}, S) h_{mn}\left(\frac{\delta+\delta_{\rm v}}{\sqrt{s}}, \frac{\delta_{\rm c}}{\sqrt{S}}, \sqrt{\frac{S}{s}}\right), \quad \text{(B1)}$$

where the h_{mn} were defined in Lam & Sheth (2009a),

$$Q_{30} = \frac{\sqrt{s-S}}{\sqrt{s}} \left[1 - \frac{(\delta_{\rm v}-\delta_{\rm c})^2}{s-S}\right]\; p_0\left(\frac{\delta_{\rm v}-\delta_{\rm c}}{\sqrt{s-S}}\right),$$

$$Q_{03} = \frac{(s-S)^2}{s^2}\, H_3(\delta_{\rm c}/\sqrt{S}) \frac{1 + {\rm erf}\left[(\delta_{\rm v}-\delta_{\rm c})/2\sqrt{s-S}\right]}{2}$$
$$+ \frac{S(s-S)(2S-3s) + \left[S^2\left(\delta_{\rm v}^2 + \delta_{\rm v}\delta_{\rm c} + \delta_{\rm c}^2\right) - 3sS\left(\delta_{\rm v}\delta_{\rm c} + \delta_{\rm c}^2\right) + 3\delta_{\rm c}^2 s^2\right]}{s^2\sqrt{S}\sqrt{s-S}}$$
$$\times\; p_0\left(\frac{\delta_{\rm v}-\delta_{\rm c}}{\sqrt{s-S}}\right), \quad \text{(B2)}$$

$$Q_{21} = -\frac{\sqrt{S}\sqrt{s-S}}{s}\left[1 - \frac{(\delta_{\rm v}-\delta_{\rm c})^2}{s-S} + \frac{\delta_{\rm c}(\delta_{\rm v}-\delta_{\rm c})}{S}\right] p_0\left(\frac{\delta_{\rm v}-\delta_{\rm c}}{\sqrt{s-S}}\right),$$

$$Q_{12} = -\frac{-sS(s-S) + \delta_{\rm v}^2 S^2 - 2\delta_{\rm v}\delta_{\rm c} sS + \delta_{\rm c}^2 s^2}{Ss^{3/2}\sqrt{s-S}}\, p_0\left(\frac{\delta_{\rm v}-\delta_{\rm c}}{\sqrt{s-S}}\right),$$

with $p_0(x) = {\rm e}^{-x^2/2}/\sqrt{2\pi}$. In addition, we may define

$$Q_3 \equiv \int_{-\infty}^{0} {\rm d}\delta\; p_0(\delta+\delta_{\rm v}, s|\delta_{\rm c}, S) H_3(\delta_{\rm c}/\sqrt{S}) = H_3(\delta_{\rm c}/\sqrt{S}) \frac{1 + {\rm erf}\left[(\delta_{\rm v}-\delta_{\rm c})/2\sqrt{s-S}\right]}{2}. \quad \text{(B3)}$$

If we again ignore the scale dependence of $\sigma\ S_3$, then

$$f(\delta_{\rm v}, s|\delta_{\rm c}, S) = 2\frac{\partial P(\delta_{\rm v}, s|\delta_{\rm c}, S)}{\partial s} = f_0(\delta_{\rm v}, s|\delta_{\rm c}, S) - 2\frac{\sigma S_3}{6}\frac{\partial}{\partial s}\left[\mathcal{E}(s,S) p_0\left(\frac{\delta_{\rm v}-\delta_{\rm c}}{\sqrt{s-S}}\right)\right], \quad \text{(B4)}$$

where $\mathcal{E}(s, S)$ is the same as in Lam & Sheth (2009a) with $b = \delta_{\rm v}$ and $B = \delta_{\rm c}$.

This paper has been typeset from a TEX/LATEX file prepared by the author.